

Raman-scattering measurements and fracton interpretation of vibrational properties of amorphous silicon

Mile Ivanda

Ruder Bošković Institute, Bijenička 54, 41000 Zagreb, Croatia

(Received 4 August 1992)

Results of Raman scattering on *a*-Si:H films are presented at frequencies from 20 to 2500 cm⁻¹. The frequency and temperature dependence of the Stokes/anti-Stokes ratio of Raman scattering intensity show the boson character of the observed broad background signal. It has been shown that the fractal model can be successfully applied to *a*-Si:H as well. The crossover frequency ω_{co1} between phonon and fracton regimes and the fractal exponent $(\sigma + d - D)\bar{d}/D$, obtained from the frequency dependence on the Raman scattering intensity, have been determined.

Fractal concepts have proved to be very successful in the interpretation of many physical phenomena in solids such as silica aerogels, polymers, and amorphous solids.¹⁻⁶ Structures that are fractal at length scales *l* intermediate between their particle size *a* and their correlation length ξ exhibit at least three distinct vibration regime modes, namely, phonon ($l > \xi$), fracton ($a < l < \xi$), and particle ($l < a$) modes.

The waves of wavelength $\lambda > \xi$ are weakly localized acoustic phonons. Because of disorder, which destroys the translation symmetry, it is possible to observe an inelastic light scattering from acoustical phonons in amorphous solids. The intensity of light scattered with a frequency shift $-\omega/2\pi$ is determined by the Raman tensor $I_{\alpha\beta,\gamma\delta}(\omega, T)$. According to Shuker and Gammon,⁷ this intensity is given by

$$I_{\alpha\beta,\gamma\delta}(\omega, T) = \frac{n(\omega, T) + 1}{\omega} \sum_b C_{\alpha\beta,\gamma\delta}^b(\omega) g^b(\omega), \quad (1)$$

where $n(\omega, T)$ is the boson thermal occupation number at equilibrium temperature *T*, $C_{\alpha\beta,\gamma\delta}^b$ is Raman coupling constant of the band *b* to the optical radiation field, the index $\alpha\beta(\gamma\delta)$ indicates the polarization of the incident (scattered) light, and $g^b(\omega)$ is the density of vibrational states of the band *b*. At low energy both $g(\omega)$ and $C(\omega)$ are proportional to ω^2 . Therefore, by introducing an extra radiation factor,⁸ the reduced Stokes Raman-scattered intensity $I^R(\omega)$ becomes

$$I^R(\omega) = \frac{I(\omega, T)}{(\omega_L - \omega)^3 [n(\omega, T) + 1]} \sim \omega^3. \quad (2)$$

With increasing the frequency ω , the fracton regime characterized by a strong localization occurs beyond a first-crossover frequency ω_{co1} (see Refs. 9 and 10). If the electric field of the incoming wave is approximately constant over the localization length *l* of the fracton, the reduced Raman intensity at frequencies $\omega \gg \omega_{\text{co1}}$, according to Stroll, Kolby, and Courtens,¹¹ is given by

$$I^R(\omega) \sim \omega^{-2[1 - (\sigma + d - D)\bar{d}/D]}, \quad (3)$$

where σ is a dimension describing the scaling of the inter-

nal length in the fractal, i.e., $s_l \sim l^\sigma$ (see Ref. 11), \bar{d} the spectral dimension,² *D* fractal or Hausdorff dimension,² and *d* the space dimension. On the frequency scale, the fractons are expected in the range from ω_{co1} to $\omega_{\text{co2}} \approx \omega_{\text{co1}}(\xi/a)^{D/\bar{d}}$ where *a* is the atomic distance which sets the shortest length scale in the fractal. Above ω_{co2} , the surface and bulk vibrational modes of particles dominate the phonon density of states.

It was shown¹ that the thermal properties of epoxy resin, glasses, and neutron-irradiated quartz could be understood on the basis of fracton excitations above and phonon excitation below a crossover frequency ω_{co1} . In addition, the so-called "boson peak" in the Raman-scattering spectra of amorphous solids is closely connected with such properties.^{12,13} In our recent paper,¹⁴ we showed that the broad background signal (BBS) observed in Raman spectra, first attributed to the recombination of nonthermal electrons with nonthermal holes,¹⁵ has properties typical for the boson peak in glasses.¹² Here, according to the temperature behavior, we will confirm the bosonlike character of the excitation, and we will show that the fractal model can be successfully applied to amorphous silicon as well.

There are several reasons to expect fractal behavior in amorphous silicon.

(a) Most *a*-Si:H films are formed by deposition processes at relatively low temperature. In that case minimum energy configurations are not attained by the solid phase; therefore, fractal aggregation such as growth of polymer chains or dendritic growth¹⁶ seems plausible.

(b) The incorporation of hydrogen may stimulate nucleation at the locations where the hydrogen is likely to bond (hydrogen clusters, polymer chain, etc.).

Furthermore, there are some experimentally observed phenomena in *a*-Si:H which are fundamentally difficult to explain by traditional models such as dispersive transport of transient photocurrents,¹⁷ a large reduction of dc dark conductivity due to incorporation of atomic hydrogen, and linear energy dependence of the electronic density of states.¹⁸ McLeod and Card¹⁹ have given a qualitatively good explanation of these phenomena in terms of fractal geometry.

Hydrogenated amorphous silicon film, about $1.3 \mu\text{m}$ thick, was prepared on no-heated silicon (111) substrates by a dc magnetron sputtering method. The sputtering was performed in a mixture of Ar and H_2 gases with partial pressures of 1.33 and 0.5 Pa, respectively. The deposition rate was $\approx 100 \text{ \AA}/\text{min}$. The hydrogen concentration, estimated by infrared spectra, was $\approx 16\%$. The excitation light for Raman scattering ($\lambda = 5145 \text{ \AA}$) was emitted from a COHERENT INNOVA 100 Ar-ion laser. The diameter of the laser beam on the sample was $\approx 100 \mu\text{m}$, and the applied laser power was 1 W. The Raman-scattered light was analyzed with a DILOR Z-24 triple spectrometer in a right-angle-scattering geometry. The spectral slit width was 9 cm^{-1} . During two scans, the scattered light was accumulated for 3 sec every 4-cm^{-1} scanning step interval. The dark count rate of the photomultiplier tube was ≈ 2.5 counts/sec, while the maximal signal of the TO-phonon-like band was ≈ 4000 counts/sec. The sample was evacuated to 10^{-4} Torr. In the low-temperature measurements, the sample was cooled with a helium closed-circle CTi CRYODYNE cryocooler up to 20 K. In order to avoid undue heating of the sample, the laser power was reduced to 200 mW, but the accumulation time of the signal was increased to 2×30 sec. The mean temperature of the exposed part of the sample was determined from the Stokes/anti-Stokes ratio at the peak intensity of the 476-cm^{-1} TO-phonon-like band of *a*-Si by the method described by Kip and Meier.²⁰ The Stokes and anti-Stokes Raman spectra were radiometrically corrected by the method of Purcell, Kaminski, and Russavage,²¹ which is described in more detail in Ref. 22.

Figure 1 displays Stokes and anti-Stokes HH- and HV-

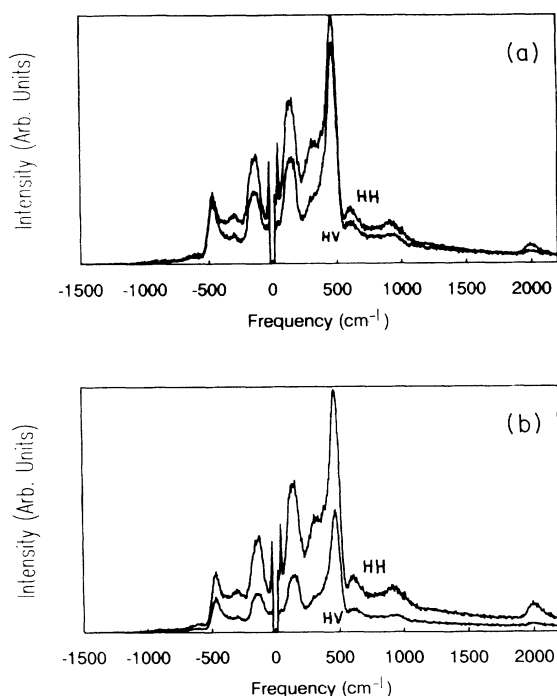


FIG. 1. Polarized Raman spectra of *a*-Si:H radiometrically (a) uncorrected and (b) corrected.

polarized Raman spectra radiometrically uncorrected [Fig. 1(a)] and corrected [Fig. 1(b)]. The polarization designation H(V) corresponds to light polarized (or analyzed) horizontally (vertically) with respect to the scattering plane. It is evident that the vibrational bands¹⁴ are superimposed on the broad background signal. To confirm the bosonlike character of the excitations in the spectral interval considered, the Stokes/anti-Stokes ratio of intensity must obey the Bose-Einstein statistics, i.e.,

$$I_S/I_{AS}(\omega, T) = \left[\frac{\omega_L - \omega}{\omega_L + \omega} \right]^3 e^{\hbar\omega/kT}, \quad (4)$$

as shown, for frequency dependence, in Fig. 2. The support of this statement is the temperature dependence of the Stokes/anti-Stokes ratio of the Raman intensity shown in Fig. 3 at frequencies 40, 140, and 250 cm^{-1} [Fig. 3(a)] and 476, 590, and 750 cm^{-1} [Fig. 3(b)]. The main part of the intensity at 40, 140, and 476 cm^{-1} belongs to the phonons of the TA- and TO-like phonon bands, while the intensity at 250, 590, and 750 cm^{-1} belongs approximately only to the BBS, which, according to our assumption, corresponds to the fractals that also obey Bose-Einstein statistics. The expected values (solid line) are in excellent agreement with the measured ones (points).

Figure 4 shows the depolarization ratio spectrum for the BBS, $\rho(\omega) = I_{HV}/I_{HH}$. It is approximately constant in the whole analyzed spectral range. The local minimums at ≈ 300 and 2000 cm^{-1} and the local maximum at $\approx 480 \text{ cm}^{-1}$ are the result of the influence of the depolarization ratio of the LA-like, SiH stretching vibrations and TO-like phonon band, respectively. While it is difficult to explain the constant value of the depolarization ratio in such a large spectral interval by homogeneous Euclidian structure, in the self-similar fractal geometry, anisotropy of the fractals is expected to be equal at all localization lengths of the fractal vibrations.¹⁰ Arguments in favor of this conclusion are supported by the results of Mazzacurati *et al.*,²³ who reported the computed depolarization ratio of the Raman intensity of fractals which slightly decrease with frequency from ≈ 0.45 to 0.33. This agrees well with our value of ≈ 0.4 in the whole fracton frequency range.

To fit the obtained intensity distribution in the curve of

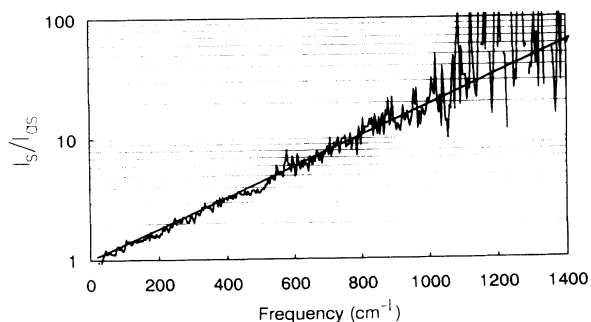


FIG. 2. Stokes/anti-Stokes ratio of the HV-polarized Raman intensity in dependence on frequency. The straight line represents the expected values according to the boson character of the excitation.

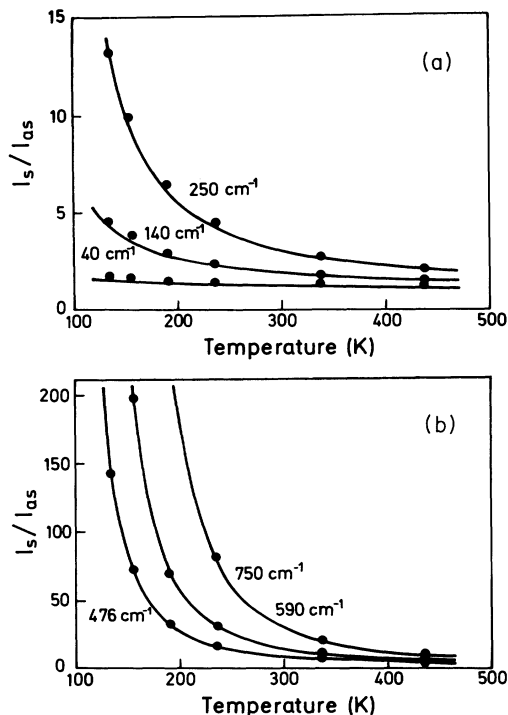


FIG. 3. Temperature dependence of Stokes/anti-Stokes ratio of HV-polarized Raman intensity at different frequencies: (a) 40, 140, and 250 cm^{-1} and (b) at 476, 590, and 750 cm^{-1} . The lines are the expected values according to the boson character of the excitation.

the BBS, we assume a continuous transition from the phonon to the fracton scattering regime. This assumption is consistent with recent measurements by Brillouin²⁴ and neutron²⁵ scattering on silica aerogels. According to the previous considerations of this problem by Yakubo, Courtens, and Nakayama (see Ref. 26 and references therein), the relation for the continuous transition would be

$$I^R(\omega) \sim \omega^3(\omega^2 + \omega_{\text{co1}}^2)^{[(\bar{d}/D)(\sigma + d - D) - 5/2]} \quad (5)$$

Actually, Eq. (5) represents a reduced Raman intensity originating simultaneously from the scattering on phonons [corresponding to Eq. (2) at $\omega \ll \omega_{\text{co1}}$], from fractons [corresponding to Eq. (3) at $\omega \gg \omega_{\text{co1}}$], and from the

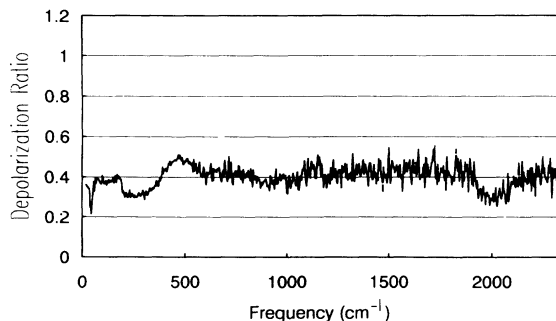


FIG. 4. Depolarization spectrum $\rho(\omega) = I_{\text{HV}}/I_{\text{HH}}$ of *a*-Si:H.

crossover frequency range, thus assuring the continuity of the whole frequency range considered.

The fitting procedure, where all parameters of the fitting curves are free, gives the correct shape of the reduced HV-polarized Raman intensity [Fig. 5(a)], with residuals better than $\pm 10\%$ [Fig. 5(b)], in the whole frequency interval considered. The fitting curve is achieved at $\omega_{\text{co1}} = 245 \text{ cm}^{-1}$ and $(\sigma + d - D)\bar{d}/D = 0.54$ for the BBS, and at values shown above Fig. 1 of the peak intensity, frequency, and bandwidth of the Gaussians which cover the phonon bands. The inset shows the reduced HV-polarized Raman spectrum (solid line) and fitted curve for the BBS (dashed line) in log-log coordinates from 20 to 6000 cm^{-1} . The fracton regime would be about order of magnitude in ω . Deviation of the signal from the fitted curve below 50 cm^{-1} is due to large-scale excitation, which appeared in most of the amorphous solids.²⁷

The correlation length corresponding to the given crossover frequency is $\xi = v/(\omega_{\text{co1}}c)$, where $v = 4.4 \times 10^5 \text{ cm/s}$ (see Ref. 28) is the average sound velocity in *a*-Si:H and c is the speed of light. That gives $\xi \approx 6 \text{ \AA}$, which shows a small fractal range in *a*-Si:H.

The fractal exponent depends on the scaling factor and fractal and spectral dimensions. In view of the simula-

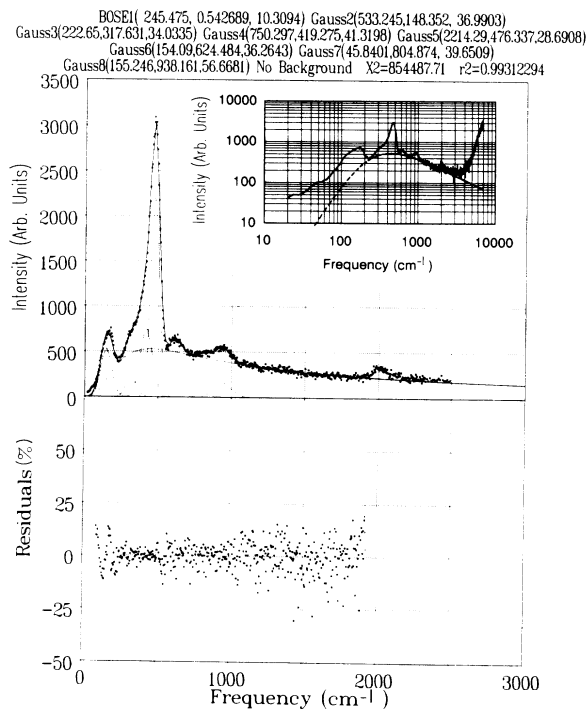


FIG. 5. (a) Reduced HV-polarized Raman intensity and fitted curve according to the fracton model. The phonon bands were taken as Gaussians with free parameters of the peak intensity, frequency, and bandwidth. Gaussians 1–8 correspond to silicon TA-, LA-, LO-, and TO-like phonon bands, silicon-hydrogen wagging and bending bond vibrations, and silicon 2TO stretching vibrations, respectively. The inset shows the reduced Raman spectrum (solid line) and fitted boson peak (dashed line) up to 6000 cm^{-1} in log-log coordinates. (b) Residual intensities from fitted curve.

tion in a recent paper of Stoll, Kolb, and Courtens,¹¹ $\sigma = 1.1$. The calculated value of the spectral dimension for the tensorial elasticity, which is mostly expected in the real world, is $\bar{d} = 0.9$ (see Ref. 29). These give, from the fitted fracton exponent, the fractal dimension $D = 2.56$, which is very close to the theoretical value $D = 2.5$ for the percolation network.³⁰ The value $D/\bar{d} = 2.85$ allows us to find $\omega_{\text{co2}} = 3300 \text{ cm}^{-1}$, which agrees well with the deviation from the fitted curve shown in the inset of Fig. 5.

In conclusion this work shows that the broad background signal or boson peak observed in the Raman spectra of *a*-Si:H behaves according to Bose-Einstein statistics. The depolarization ratio and shape of the signal are

well explained by the existence of fractals. Such a fractal analysis enables us to find the density of the vibrational states which determine the thermal and transport properties of either *a*-Si:H or amorphous solids generally. Nevertheless, whether one does or does not accept the phonon-fracton hypothesis for the explanation of the boson peak, its presence in *a*-Si:H is unequivocal and, because of the simple tetrahedral structure of *a*-Si, can be of help in investigation of the boson peak in other amorphous solids.

We thank Dr. L. Colombo for a critical reading of the manuscript.

-
- ¹S. Alexander, C. Laermans, R. Orbach, and H. M. Rosenberg, Phys. Rev. B **28**, 4615 (1983).
²E. Courtens, R. Vacher, and E. Stoll, Physica D **38**, 41 (1989).
³R. Kopelman, S. Parus, and J. Prasad, Phys. Rev. Lett. **56**, 1742 (1986).
⁴R. Vacher, E. Courtens, G. Coddens, J. Pelous, and T. Woignier, Phys. Rev. B **39**, 7384 (1989).
⁵Y. Termonia, J. Stat. Phys. **36**, 1356 (1984).
⁶L. Niemeyer, L. Pietronero, and H. J. Weismann, Phys. Rev. Lett. **52**, 1033 (1984).
⁷R. Shuker and R. W. Gammon, Phys. Rev. Lett. **25**, 222 (1970).
⁸W. Hayes and R. Loudon, *Scattering of Light by Crystals* (Wiley, New York, 1978), p. 26.
⁹Y. Tsujimi, E. Courtens, J. Pelous, and R. Vacher, Phys. Rev. Lett. **60**, 2757 (1988).
¹⁰S. Alexander, Phys. Rev. B **40**, 7953 (1989).
¹¹E. Stoll, M. Kolb, and E. Courtens, Phys. Rev. Lett. **68**, 2472 (1992).
¹²V. K. Malinovsky, V. N. Novikov, P. P. Parshin, A. P. Sokolov, and M. G. Zemljanov, Europhys. Lett. **11**, 43 (1990).
¹³S. R. Elliot, Europhys. Lett. **19**, 201 (1992).
¹⁴M. Ivanda, K. Furić, O. Gamulin, and D. Gracin, J. Non-Cryst. Solids **137&138**, 103 (1991).
¹⁵I. H. Campbell, P. M. Fauchet, S. A. Lyon, and R. J. Nemanich, Phys. Rev. B **41**, 9871 (1990).
¹⁶R. F. Voss and M. Tankiewicz, J. Electrochem. Soc. **132**, 371 (1985).
¹⁷J. Shirafuji and Y. Inushi, in *Amorphous Semiconductor Technologies and Devices*, edited by Y. Hamakawa (North-Holland, Tokyo, 1983), Vol. 6, p. 47.
¹⁸W. B. Jackson, S. J. Oh, C. C. Tsai, and J. W. Allen, Phys. Rev. Lett. **53**, 1481 (1984).
¹⁹R. D. McLeod and H. C. Card, J. Non-Cryst. Solids **105**, 17 (1988).
²⁰B. J. Kip and R. J. Meier, Appl. Spectrosc. **44**, 707 (1990).
²¹F. J. Purcell, R. Kaminski, and E. Russavage, Appl. Spectrosc. **34**, 323 (1980).
²²M. Ivanda and K. Furić (unpublished).
²³V. Mazzacurati, M. Montanaga, O. Pilla, G. Vilianni, G. Ruocco, and S. Signorelli, Phys. Rev. B **45**, 2126 (1992).
²⁴E. Courtens, C. Lartique, F. Mezeli, R. Vacher, G. Coddens, M. Foret, J. Pelous, and T. Woignier, Z. Phys. B **79**, 1 (1990).
²⁵R. Vacher, E. Courtens, G. Coddens, A. Heidemann, Y. Tsujimi, J. Pelous, and M. Foret, Phys. Rev. **65**, 1008 (1990).
²⁶K. Yakubo, E. Courtens, and T. Nakayama, Phys. Rev. B **42**, 1078 (1990).
²⁷R. J. Nemanich, Phys. Rev. B **16**, 1655 (1977).
²⁸L. R. Testardi and J. J. Hauser, Solid State Commun. **21**, 1039 (1977).
²⁹I. Webman and G. S. Grest, Phys. Rev. B **31**, 1689 (1985).
³⁰S. Alexander and R. Orbach, J. Phys. (Paris) Lett. **43**, L625 (1982).